DOI: 10.61782/fa.2025.0908

FORUM ACUSTICUM
EURONOISE 2025

TOWARDS PLASMACOUSTIC METAMATERIALS

Han Miao[1] **Stanislav Sergeev**[2] **Rahim Vesal**[1] **Hervé Lissek**[1*]
[1]Laboratory of Wave Engineering, Ecole Polytechnique Fédérale de Lausanne, Switzerland
[2]Sonexos SA, Route de la Grotte 6, CH-1003 Lausanne, Switzerland

ABSTRACT

The ”plasmacoustic metalayer” concept relies on the use of a Corona Discharge Transducer (CDT), transparent towards fluid flows and to light. When used as an actuator within an active control system, it allows manipulating sound waves in transmission/reflection/absorption without resorting to a membrane or any other mechanical intermediate, contrarily to conventional loudspeakers. Moreover, owing to its non-resonant nature, the CDT is an obvious candidate for the development of broadband active acoustic metamaterials, especially since it is transparent to sound in a ”passive” mode.

This presentation aims to showcase some examples of active plasmacoustic metamaterials concepts, through numerical simulations and experimental validations, at the unit-cell level. These preliminary results will allow drawing conclusions on the applicability of the CDT to achieve broadband active acoustic metamaterials, and identifying routes for further development of the concept.

Keywords: acoustic metamaterials, plasmacoustic metalayers, active control

1. INTRODUCTION

Acoustic metamaterials have emerged in the early 2000's inspired by the literature on their electromagnetic counterparts. In its general definition, an acoustic metamaterial is an artificial structure consisting of miniature engineered elements (cavities, ducts, membranes, etc.), assembled in such a way so that the whole exhibits physical properties that mimic or even go beyond physical phenomena occurring in nature. The most important feature of these unit-cells is their subwavelength dimension, namely their size should much smaller than the wavelengths they interact with [1].

However, most of the reported architectures rely on resonant structures (Helmholtz resonators, coiled-space cavities, membranes) [2–4]. Therefore, the resulting anomalous/negative properties are limited to a narrow frequency bandwidth, if not at a single frequency. Also, their inherent losses negatively impact their “transmissibility” capacities (the amount of acoustic energy that can be effectively transmitted “forward” by the artificial structure), and therefore preclude any practical application. More generally, passive linear metamaterials are bound to the Kramers-Kronig relations, eventually leading to trade-offs in terms of bandwidth of operation and transmissibility.

In a view to overpassing the inherent limitations of passive structures, active acoustic metamaterial concepts have been recently investigated. In this paradigm, the unit-cells are composed of electroacoustic transducers (loudspeakers and microphones) connected by a control platform, in a view to adapting their dynamic response to ongoing sound waves. Thanks to such a tunability, it is possible to observe exotic time-varying properties such as time-reversal for sound focusing, non-Hermitian media, acoustic circulators, acoustic diodes, and many other interesting topological phenomena, that were not possible with passive constructions. But conventional loudspeakers are still intherently resonant, thus limited in terms of bandwidth of operation, and more importantly, they are prone to introduce significant losses against which the control should devote a significant par of energy to function. Last, they rely on (opaque) membrane radiators, that cannot avoid scattering (loudspeakers are obstacles to the propagation of sound in a metamaterial structure).

The Plasmacoustic Metalayer recently developed by

*__Corresponding author__: herve.lissek@epfl.ch.

Sergeev et al [6, 7] allows interacting with exogenous sound waves in a membraneless manner, thanks to a Corona Discharge Transducer (CDT) [5]. Besides its almost transparency to fluid flows (and light), which makes it non-scattering and lossless in its passive form, the main asset for metamaterial applications is its non-resonant characteristics. In active mode, it has been capable to exhibit almost ideal sound absorption over an ultrabroadband frequency range (20 Hz-2000 Hz), owing to the absence of mechanical interface known to bound the bandwidth of operation in conventional loudspeaker-based active control systems. Moreover, further use of the concept in transmission configuration have been demonstrated, showing also variable broadband reflection/transmission modules and phases. This makes the Plasmacoustic Metamalayer a most promising candidate as unit-cell for active metamaterial applications.

This paper introduces the Plasmacoustic Metamaterial (PM) concept, by leveraging some examples of active sound reflection/transmission results achieved by the plasmacoustic metalayer concept. These examples will be discussed in the light of their application as plasmacoustic metamaterial unit-cells (PMUC), that are the heart of a research project submitted for funding to the Swiss National Science Foundation.

2. THE CORONA-DISCHARGE ELECTROACOUSTIC TRANSDUCER

2.1 Corona discharge transducer in a "wire-to-grid" configuration

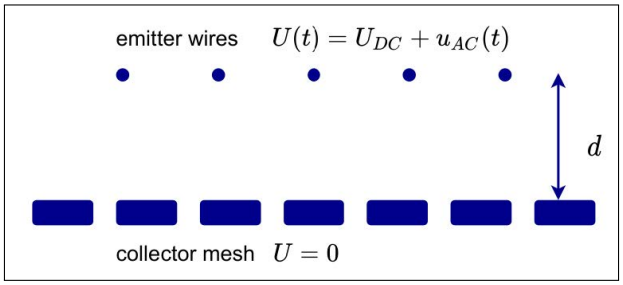

Figure 1. Sketch representing a cut view of the electrode pair: corona electrode (emitter wires)/collector electrode (grounded perforated grid)

Corona discharge transducers (CDT) allow for sound generation due to the ionization of molecules in the surrounding fluid, moved by an intense oscillating electric field. In the "wire-to-grid" configuration, the transducer is constituted by a pair of electrodes (forming two parallel planes, as illustrated in the sketch of Fig. 1): the first one is a perforated metallic grid connected to the ground, and is designated the "collector electrode"; the second one, designated "corona electrode", is made of an ultra thin wire (diameter of the order of 100 μm), arranged in a pattern of parallel lines along a same plane parallel and distant of d to the collector plane, put at a sufficiently high voltage so as to trigger the extraction of electrons from surrounding molecules. The breakdown voltage, above which ionization is possible, is designated U_0 and is of the order of a few kV.

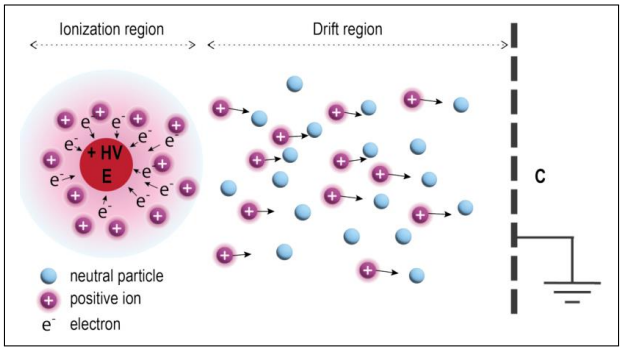

Figure 2. Corona discharge principle

When applying an offset voltage U_{DC} higher than U_0, positive ions are accelerated inside the ionization region towards the collector electrode. They then collide with the neutral particles present in the drift region, which are then moved, giving rise to an "ionic wind" (constant flow).

If an alternating voltage $u_{ac}(t)$, of the order of 1 kV, is superimposed to U_{DC} (while total voltage $U_{DC} + u_{ac}$ still remains higher than the breakdown voltage, as well as not exceeding a value above which arcing may occur), the transducer generates acceleration/deceleration of the surrounding fluid layers, responsible for sound generation.

The preceding studies show that this corona discharge transducer configuration could be modelled as the combination of two volumic sound sources, one monopolar "heat" source H (due to the heat release at the corona electrodes), and another dipolar "force" source F (relative to the electrostatic force moving the surrounding fluid back and forth).

An extremely simple electroacoustic model can be deduced from the coupling equations between the plasma generation and actuation, and the generated sound field.

Indeed, it has been shown that the offset voltage U_{DC} can be linked to the current I flowing through the corona wire according to the Townsend formula:

$$I = CU_{DC}(U_{DC} - U_0) \tag{1}$$

where C is a constant that depends on the transducer geometry, and that can be experimentally determined. It is then possible to express the two sources H and F as a function of the voltage feeding the transducer [5, 6]:

$$\begin{aligned} H &= C(3U_{DC}^2 - U_{DC}U_0)u_{ac}\ [\mathrm{W}] \\ F &= \frac{C.d}{\mu_i}(2U_{DC} - U_0)u_{ac}[\mathrm{N}] \end{aligned} \tag{2}$$

where μ_i designates ions mobility, and d is the distance between the two electrodes (or the plasma thickness). It can be seen that the two sound sources are interdependent. Their individual influence is independent on frequency but on the constant parameters U_0, U_{DC}, C, d and μ_i, and not directly on the transducer cross-section area S. However, the lateral dimensions of the CDT is likely to change the current-voltage law (Eq. (1)), thus C.

In the following, we define the the heat source power density $h = \frac{H}{S.d}$ (in W/m^3), and the dipolar force source density $f = \frac{F}{S.d}$ (in N/m^3), where S is the transducer effective cross-section area, to be used in the expression of the sound fields generated by the CDT.

3. THE PLASMACOUSTIC METALAYER AS A METAMATERIAL UNIT-CELL

Let's consider a 1D waveguide along dimension x being the host of the PMUC, as illustrated in Fig. 3. In the PM paradigm, we will consider a unit-cell integrating a CDT, one ore more microphones (either one on the front side when backed by a rigid cavity, or with at least 2 microphones, one on each sides of the transducer in an open configuration), a control hardware and a power amplifier capable to manage the high voltage DC and the acoustic control voltage u_{ac}, as illustrated on Fig. 3. For the sake of simplicity, the controller part includes the power amplifier, to deliver a given voltage u_{ac} to the transducer.

In the configuration where the CDT is centered at the origing $x = 0$ and oriented so that the collector electrode is located towards the left (with respect to the chosen direction of axis x of the waveguide) and the corona electrode being on the right side, a given ac voltage u_{ac} will give rise to a dipolar force source that will generate out-of-phase (wrt. u_{ac}) sound pressures towards the increasing x direction, while generating in-phase (wrt. u_{ac}) sound pressures towards the decreasing x direction. The different contribnutions to the acoustic field generated by the CDT will then be (distinguised between negative and positive x half-domains):

$$\text{for } x < 0 : \begin{cases} p_h(x) = \dfrac{dc_0}{2C_pT_0}he^{jkx} \\ p_f(x) = \dfrac{d}{2}fe^{jkx} \\ v_h(x) = -\dfrac{d}{2\rho_0C_pT_0}he^{jkx} \\ v_f(x) = -\dfrac{d}{2\rho_0c_0}fe^{jkx} \end{cases} \tag{3}$$

$$\text{for } x > 0 : \begin{cases} p_h(x) = \dfrac{dc_0}{2C_pT_0}he^{-jkx} \\ p_f(x) = -\dfrac{d}{2}fe^{-jkx} \\ v_h(x) = \dfrac{d}{2\rho_0C_pT_0}he^{-jkx} \\ v_f(x) = -\dfrac{d}{2\rho_0c_0}fe^{-jkx} \end{cases} \tag{4}$$

If we consider an exogenous sound field $p_{ac}(x) = p_{ac}^+e^{-jkx} + p_{ac}^-e^{+jkx}$, and the associated particle velocity $v_{ac}(x) = \frac{1}{\rho_0c_0}\left(p_{ac}^+e^{-jkx} - p_{ac}^-e^{+jkx}\right)$, we can derive the total pressure fields on both sides of the unit-cell as:

$$x < 0 : \begin{cases} p_t(x) = p_{ac}^+e^{-jkx} \\ \qquad + \left(p_{ac}^- + \dfrac{dc_0}{2C_pT_0}h + \dfrac{d}{2}f\right)e^{jkx} \\ v_t(x) = \dfrac{1}{\rho_0c_0}\left[p_{ac+}e^{-jkx}\right. \\ \qquad \left. - \left(p_{ac}^- + \dfrac{dc_0}{2C_pT_0}h + \dfrac{d}{2}f\right)e^{jkx}\right] \end{cases} \tag{5}$$

$$x > 0 : \begin{cases} p_t(x) = p_{ac}^-e^{jkx} \\ \qquad + \left(p_{ac}^+ + \dfrac{dc_0}{2C_pT_0}h - \dfrac{d}{2}f\right)e^{-jkx} \\ v_t(x) = \dfrac{1}{\rho_0c_0}\left[-p_{ac}^-e^{jkx}\right. \\ \qquad \left. + \left(p_{ac}^+ + \dfrac{dc_0}{2C_pT_0}h - \dfrac{d}{2}f\right)e^{-jkx}\right] \end{cases} \tag{6}$$

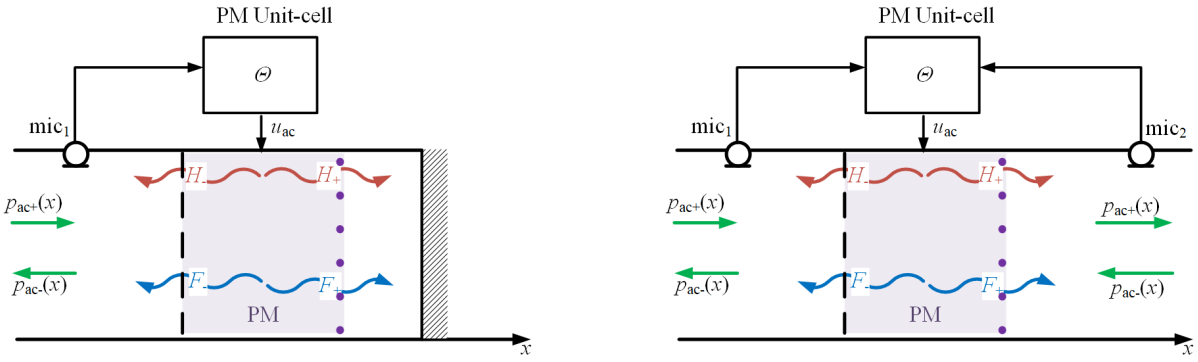

Figure 3. Realizations of a PMUC in a 1D waveguide: left: PMUC backed by a rigid termination; right: PMUC open on both sides

In these sets of equations, h and f are intricate as they both depend on u_{ac}. Still, the control of u_{ac} as a function of one ore more microphone inputs allows achieving interesting acoustic properties over the PMUC. The following section intends to present some of the applications.

4. EXAMPLES OF PLASMACOUSTIC METAMATERIAL UNIT-CELL REALIZATIONS

4.1 PMUC in reflection

The first realization of a PMUC in reflection is reported in [6]. In this experience, the PMUC is in the backed configuration (see Fig. 3-left), with a control microphone located at position $-x_0$ (the PMUC center being at the origin $x = 0$). In this configuration, the left-handed side of the PMUC can simplify, taking into account the reflection at the back wall distant of l from the PMUC center. Accounting for the actual (measurable) specific impedance $Z_l = \frac{p_t(x=l)}{v_t(x=l)}$ at the wall ($x = l$), we derive the reflection coefficient $R = \frac{Z_l - Z_c}{Z_l + Z_c}$ and then the relationships on the left side ($x < 0$) become:

$$\begin{cases} p_t(x) = p_{ac}^+ e^{-jkx} + \Big(R p_{ac}^+ \\ \quad + \dfrac{dc_0}{2C_pT_0}(1 - Re^{-2jkl})h \\ \quad + \dfrac{d}{2} f(1 - Re^{-2jkl})\Big)e^{jkx} \\ v_t(x) = \dfrac{1}{\rho_0 c_0}\Big[p_{ac}^+ e^{-jkx} - \Big(R p_{ac}^+ \\ \quad + \dfrac{dc_0}{2C_pT_0}(1 + Re^{-2jkl})h \\ \quad + \dfrac{d}{2}(1 - Re^{-2jkl})f\Big)\, e^{jkx}\Big] \end{cases} \tag{7}$$

By prescribing a target specific impedance $Z_t(-x_0) = \frac{p_t(-x_0)}{v_t(-x_0)}$ at the control microphone position, we can deduce the transfer function $\Theta(\omega) = \frac{u_{ac}}{p_t(-x_0)}$ to drive the PMUC in order to achieve the targeted impedance:

$$\begin{cases} \Theta(\omega) = \dfrac{1}{A}\dfrac{Z_c}{Z_t}\left(\dfrac{Z_t - Z_{ac}(-x_0)}{Z + Z_{ac}(-x_0)}\right) \\ A = \dfrac{d}{2}\left(f + \dfrac{c_0 h}{C_p T_0}\right)e^{-jkx_0} \\ \quad + \dfrac{d}{2}\left(\dfrac{c_0 h}{C_p T_0} - f\right)Re^{-jk(x_0+2l)} \\ Z_{ac}(-x_0) = \dfrac{p_{ac}(-x_0)}{v_{ac}(-x_0)} \end{cases} \tag{8}$$

In this study, we target a control in reflection with adjustable amplitude and phase, the target impedance being set so as to achieve target reflection coefficient $R_t =$

$|R_t|e^{j\angle(R_t)}$. In that view, we define a dimensionless factor $\zeta \in [01]$ to define a virtual acoustic termination ζZ_l, and a virtual depth of the cavity $l + \Delta l$ leading to an additional delay in the control loop. In this control strategy, the target impedance becomes:

$$Z_t = Z_c \frac{\zeta Z_l + jZ_c \tan(k(l + x_0 + \Delta l))}{Z_c + j\zeta Z_l \tan(k(l + x_0 + \Delta l))} \quad (9)$$

An experimental prototype of PMUC in absorption has been built with lateral dimensions $50\,\mathrm{mm} \times 50\,\mathrm{mm}$ and inter-electrode gap of $6\,\mathrm{mm}$, and placed in a rectangular tube of same cross-section and length $1.1\,\mathrm{m}$, with a back cavity length l =15 mm. The PCB 130D20 quarter-inch ICP microphone used for the control is located at position $x_0 = -10\,\mathrm{mm}$ and input a Speedgoat IO-334 working at $50\,\mathrm{kHz}$. Finally a TREK 615-10 high voltage AC/DC amplifier drives the PMUC with amplification gain of 1000 (accounted for in the transfer function Θ).

The reflection coefficient is measured after ISO 10534-2 standard [12], with two PCB 130D20 ICP microphones distant of $50\,\mathrm{mm}$ from each others, the signals of which are processed by a B&K Pulse Multichannel Analyzer to estimate the transfer functions H_{12} and derive the reflection coefficient in the different control cases.

We measured the reflection coefficient (in amplitude and phase) for two scenarios: one where we set the coefficient ζ to achieve different reflection amplitude of [0.9 0.7 0.4] while keeping $\Delta l = 0\,\mathrm{m}$ (see Fig. 4), and another where we keep the reflection amplitude to 0.4 while adding a virtual cavity depths of [3.7 cm, 9.7 cm, 14.7 cm], namely by adding a delay of [0.22 ms, 0.56 ms, 0.85 ms] (see Fig. 5).

We can then assign any reflection coefficient amplitude and phase to the PMUC in the backed configuration, which gives a unique possibility to control the reflection gratings over a 2D metasurface with an ultra-thin unit-cell (in the range of $1\,\mathrm{cm}$ in the current prototype, but it can be made even thinner), without having to employ acoustic or mechanical resonators with frequency-dependent thickness as reported in the current literature (space-coiling channels [8], Helmholtz resonators [9], or membrane-capped cavities [10]).

4.2 PMUC in transmission

Preliminary investigations on the use of a PMUC in open configuration for active noise reduction have been recently undertaken. In this study, the PMUC consists of a square

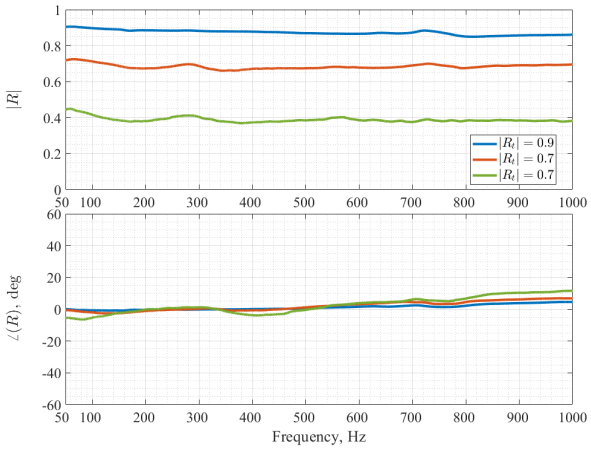

Figure 4. Reflection coefficient measured on the PMUC in an impedance tube with variable amplitude, while the phase is set to 0 degree (source: Sergeev et al [6])

CDT of size $50\,\mathrm{mm} \times 50\,\mathrm{mm}$ and inter-electrodes gap $d = 6\,\mathrm{mm}$, surrounded by two PCB 130D20 quarter-inch ICP microphones as control microphones, distant of x_0 to the center of the CDT. The PMUC is inserted in the middle of an impedance tube with same square cross-section and total length $2\,\mathrm{m}$. One extremity is loaded with a $500\,\mathrm{mm}$ long melamin wedge to ensure anechoic condition, the other hosting a loudspeaker used as the sound source. The PMUC is controlled with a Speedgoat Baseline Real-Time Target Machine to assign the targeted control law. The acoustic properties of the PMUC are measured with two pairs of PCB 378B02 half-inch ICP microphones, the signals and the transfer functions being processed with a 4-channels B&K Pulse Sound and Vibration Analyzer. The Transfer Matrix Method [13] is employed to derive the PMUC transmission properties, such as the effective propagation constant $\gamma = \alpha + j\beta$, transmission loss, or the effective impedance matrix of the small insertion of size $d + 2x_0$.

In this study, the control strategy consisted in synthesizing a target 2-port acoustic circuit comprising a series impedance Z_t, following the same methodology as the one employed for the PMUC with back-cavity configuration. Here it is important to stress on the fact that the PMUC will result in both series impedance and shunt admittance Y_t since the monopolar and dipolar sound

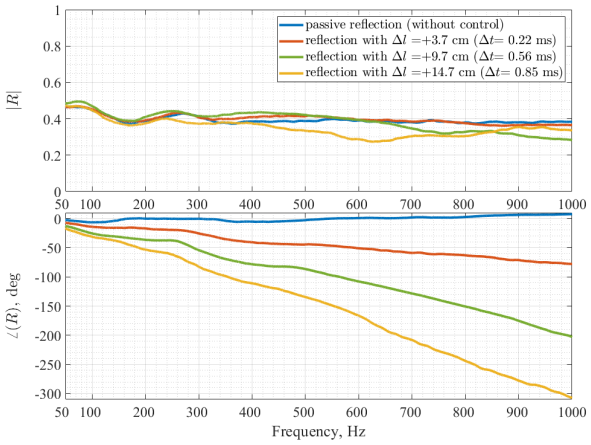

Figure 5. Reflection coefficient measured on the PMUC in an impedance tube with variable delays (source: Sergeev et al [6])

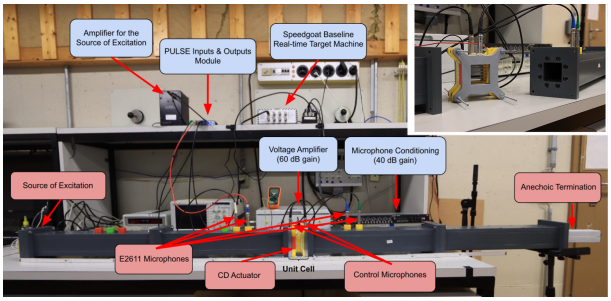

Figure 6. Setup of the PMUC assessment in transmission

sources are intricated. Nevertheless the choice has been made here to ignore the shunt admittance and verify that the control still allows achieving the series impedance, and see how much it is impacted by the resulting admittance. Therefore, the heat source h is set to 0 in the sound field expressions of Eqs. (5) and (6), in order to derive the target control law $\Theta(\omega)$, so as to deliver a prescribed particle velocity as $v_t = \dfrac{p_t(-x_0) - p_t(+x_0)}{Z_t}$.

We decided to assign two target impedances here. The first one corresponds to a layer of porous material wth porosity of 0.75 and flow resistance $1.5\,\mathrm{MPa\,s\,m^{-4}}$ and of thickness $d + 2x_0 = 64\,\mathrm{mm}$, modeled as series resistance R_t (also taking into account the "natural" mass of air $M_p = \rho_0(d + 2x_0)$ without the PMUC, while neglecting the "natural" compliance). The second one targets a single-degree-of-freedom resonator consisting of an acoustic mass M_t and compliance C_t (also taking into account the "natural" mass of air without the PMUC, while neglecting the "natural" compliance). The target impedance in these two cases are

$$\begin{cases} Z_{t,\text{porous}} = R_t + j\omega M_p \\ Z_{t,\text{membrane}} = j\omega(M_p + M_t) + \dfrac{1}{j\omega C_t} \end{cases} \tag{10}$$

where $M_p = 76.8\,\mathrm{g\,m^{-2}}$, $R_t = 0.1\,\mathrm{Pa\,s\,m^{-3}}$, M_t =331 $\mathrm{g\,m^{-2}}$ and $C_t = 6.510^{-6}\ \mathrm{m^{-1}\ N^{-1}}$. The results in terms of achieved normalized impedance $z = \frac{Z}{Z_c}$ are represented on Fig. 7 and Fig. 8.

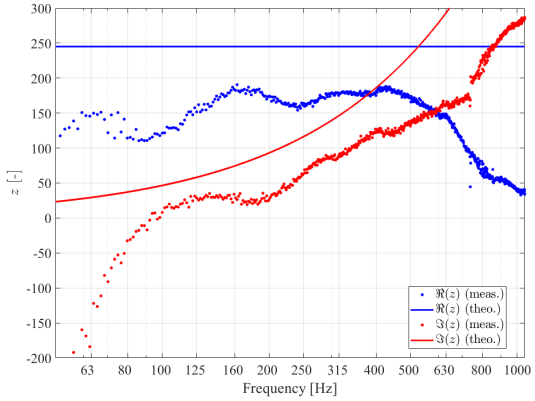

Figure 7. Normalized acoustic impedance (blue: real part; red: imaginary part) when targeting a porous layer (points: measurements; lines: target)

We can observe that the achieved impedance differs from the target one, mainly due to the assumption after which the the CDT is mainly dipolar. However, the behaviour at low frequencies fits reasonably well the target in the second case, while the achieved resistance of the first case is significantly lower than the target. The effect of the monopolar source explains the mismatch with the target, especially at high frequencies.

From these measurements, it is also possible to derive the transmission loss $TL = 10.\log_{10}\left(\dfrac{I_i}{I_t}\right)$ and the propagation contant $\gamma = \alpha + j\beta$. The examples for the case where the target impedance is the one of a porours layer are given in Fig. 9 and Fig. 10

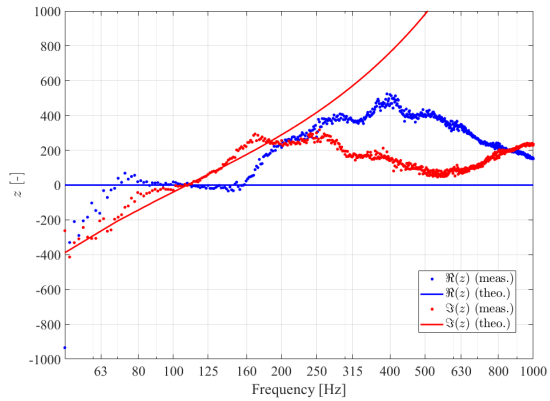

Figure 8. Normalized acoustic impedance (blue: real part; red: imaginary part) when targeting a membrane (points: measurements; lines: target)

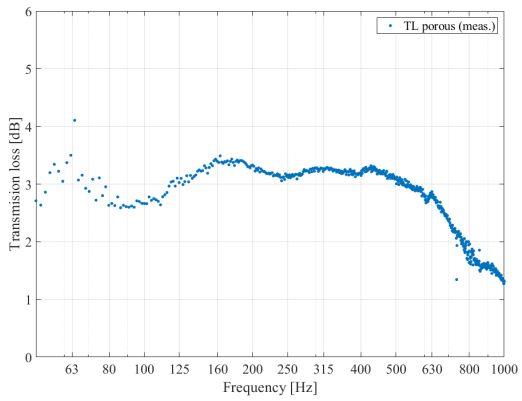

Figure 9. Transmission loss when targeting a porous layer $Z_t = R_t + j\omega M_p$

5. CONCLUSION AND PERSPECTIVES

We have shown that the PMUC allows achieving a wide range of acoustic properties, either in reflection when backed with a closed cavity, or in transmission when open on both ends. The achieved performance is aligned with the targeted one in the case where the PMUC is closed at one side, but differs in the open configuration, due to the intrication of monopolar/dipolar sound sources.

In a follow-up study, we will develop alternative control strategies that allow separating monopolar and dipolar components of the CDT, thus enabling full control on the 2-ports acoustic properties.

6. REFERENCES

[1] S.A. Cummer, J. Christensen, A. Alù, Controlling sound with acoustic metamaterials. *Nat. Rev. Mater.*, 1:16001, 2016.

[2] N. Fang, Ultrasonic metamaterials with negative modulus. *Nat. Mater.*, 5:452–456, 2006.

[3] C. Zhang, X. Hu, Three-Dimensional Single-Port Labyrinthine Acoustic Metamaterial: Perfect Absorption with Large Bandwidth and Tunability. *Phys. Rev. Appl.*, 6:064025, 2016.

[4] S. Lee, C.M. Park, Y.M. Seo, Z.G. Wang, C.K. Kim, Composite Acoustic Medium with Simultaneously Negative Density and Modulus. *Phys. Rev. Lett.*, 104:054301, 2010.

[5] S. Sergeev, H. Lissek, A. Howling, I. Furno, G. Plyushchev, and P. Leyland, Development of a plasma electroacoustic actuator for active noise control applications *Journal of Physics D: Applied Physics*, 53:495202, 2020.

[6] S. Sergeev, Plasma-based Electroacoustic Actuator for Broadband Sound Absorption, EPFL PhD Thesis N. 9784, Lausanne, Switzerland, 2022.

[7] S. Sergeev, Ultrabroadband sound control with deep-subwavelength plasmacoustic metalayers *Nat. Commun.*, 14:2874, 2023.

[8] N. Jiménez, V. Romero-García,L- M. García-Raffi, F. Camarena, K. Staliunas, Sharp acoustic vortex focusing by Fresnel-spiral zone plates. *Appl. Phys. Lett.*, 112: 204101, 2018.

[9] N. Jiménez, T. J. Cox, V. Romero-García,J. P. Groby Metadiffusers: Deep-subwavelength sound diffusers. *Sci Rep* 7: 5389, 2017.

[10] H. Esfahlani, S. Karkar, H. Lissek, J. R. Mosig, Acoustic carpet cloak based on an ultrathin metasurface. *Phys. Rev. B* 94(9):014302, 2016.

[11] F. Bongard, H. Lissek, J. R. Mosig. Acoustic transmission line metamaterial with negative/zero/positive refractive index. *Phys. Rev. B*, 82(9):094306, 2010.

[12] ISO 10534-2:2023. Determination of acoustic properties in impedance tubesPart 2: Two-microphone technique for normal sound absorption coefficient and normal surface impedance, ISO standards, 2023.

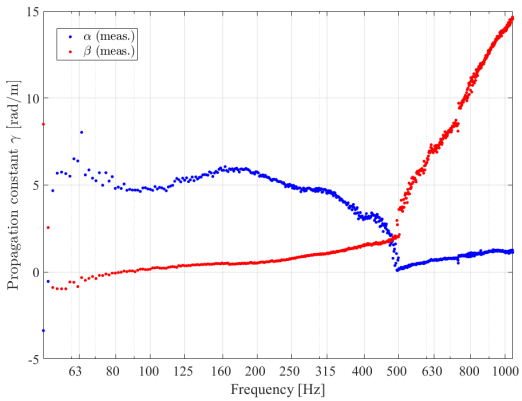

Figure 10. Propagation constant when targeting a porous layer $Z_t = R_t + j\omega M_p$

[13] ASTM 2611-19. Standard Test Method for Normal Incidence Determination of Porous Material Acoustical Properties Based on the Transfer Matrix Method, ASTM standards, 2019